doi:10.1016/j.jmb.2011.11.014 J. Mol. Biol. (2012) 415, 248–262

Contents lists available at www.sciencedirect.com

Journal of Molecular Biology

journal homepage: http://ees.elsevier.com.jmb

Altered Strand Transfer Activity of a Multiple-Drug-Resistant Human Immunodeficiency Virus Type 1 Reverse Transcriptase Mutant with a Dipeptide Fingers Domain Insertion

Laura A. Nguyen[1], Waaqo Daddacha[2], Sean Rigby[3], Robert A. Bambara[3] and Baek Kim[2]*

[1]*Department of Pathology and Laboratory Medicine, University of Rochester Medical Center, Rochester, NY, USA*
[2]*Department of Microbiology and Immunology, University of Rochester Medical Center, 601 Elmwood Avenue, Box 672, Rochester, NY 14642, USA*
[3]*Department of Biochemistry and Biophysics, University of Rochester Medical Center, Rochester, NY, USA*

Received 15 July 2011; received in revised form 1 November 2011; accepted 6 November 2011
Available online 12 November 2011

Edited by J. Karn

Keywords:
HIV-1;
reverse transcriptase;
multiple drug resistance;
fingers domain insertion;
strand transfer

Prolonged highly active anti-retroviral therapy with multiple nucleoside reverse transcriptase inhibitors for the treatment of patients infected with human immunodeficiency virus type 1 (HIV-1) can induce the development of an HIV-1 reverse transcriptase (RT) harboring a dipeptide insertion at the RT fingers domain with a background thymidine analog mutation. This mutation renders viral resistance to multiple nucleoside reverse transcriptase inhibitors. We investigated the effect of the dipeptide fingers domain insertion mutation on strand transfer activity using two clinical RT variants isolated during the pre-treatment and post-treatment of an infected patient, termed pre-drug RT without dipeptide insertion and post-drug RT with Ser-Gly insertion, respectively. First, the post-drug RT displayed elevated strand transfer activity compared to the pre-drug RT, with two different RNA templates. Second, the post-drug RT exhibited less RNA template degradation than the pre-drug RT but higher polymerization-dependent RNase H activity. Third, the post-drug RT had a faster association rate (k_{on}) for template binding and a lower equilibrium binding constant K_d for the template, leading to a template binding affinity tighter than that of the pre-drug RT. The k_{off} values for the pre-drug RT and the post-drug RT were similar. Finally, the removal of the dipeptide insertion from the post-drug RT abolished the elevated strand transfer activity and RNase H activity, in addition to the loss of azidothymidine resistance. These biochemical data suggest that the dipeptide insertion elevates strand transfer activity by increasing the interaction of the RT with the RNA donor template, promoting cleavage that generates more invasion sites for the acceptor template during DNA synthesis.

*Corresponding author. E-mail address: baek_kim@urmc.rochester.edu.

Abbreviations used: HIV-1, human immunodeficiency virus type 1; RT, reverse transcriptase; NRTI, nucleoside reverse transcriptase inhibitor; NNRTI, non-nucleoside reverse transcriptase inhibitor; HAART, highly active anti-retroviral therapy; TAM, thymidine analog mutation; AZT, azidothymidine; WT, wild type; AZTTP, 3′-azido-3′-deoxy-thymidine-5′-triphosphate; AZTMP, 3′-azido-3′-deoxythymidine monophosphate; T/P, template/primer; dTTP, thymidine triphosphate; EDTA, ethylenediaminetetraacetic acid.

Introduction

Currently, there are more than 17 anti-human immunodeficiency virus type 1 (HIV-1) drugs that have been clinically approved for the treatment of HIV-1-infected patients.[1] These anti-HIV drugs belong to six different classes, which include the most widely used anti-HIV-1 inhibitors targeting HIV-1 reverse transcriptase (RT), nucleoside reverse transcriptase inhibitors (NRTIs), and non-nucleoside reverse transcriptase inhibitors (NNRTIs).[1] Even with the advent of combination drug therapy [highly active anti-retroviral therapy (HAART)], the emergence of HIV-1 drug-resistant mutations remains an issue due to the high capability of HIV-1 to mutate and escape drug efficacy.[1–3]

The low-fidelity error-prone nature of HIV-1 replication provides the virus with numerous genomic mutations, which are mixed by frequent recombination events between two single-stranded HIV-1 RNA genomes during reverse transcription.[2–7] This leads to an enhanced ability of HIV-1 to accumulate viral mutations, rendering resistance to the applied anti-HIV-1 agents.[5,8,9] Therefore, recombination may allow the virus to efficiently combine individual pre-existing drug-resistant mutations encoded in separate viral genomes for the generation of an HIV-1 variant that is multiple-drug-resistant.[5,9–11] Adding to these problems, HAART selects a particular RT population harboring multiple genomic mutations, which yields simultaneous cross-resistance to similar types of HIV-1 drugs used, leaving fewer choices for further anti-viral treatment.[12,13]

A particular group of clinical HIV-1 RT variants that causes viral resistance to multiple NRTIs contains RT mutations with dipeptide insertions at the β3–β4 fingers domain of HIV-1 RT along with background thymidine analog mutation (TAM).[8,14–16] The T69S substitution mutation generally appears in combination with an inserted dipeptide (typically Ser and Gly) between positions 69 and 70, respectively.[16–21] Several biochemical studies have shown that dipeptide insertion, along with background TAM, is capable of unblocking primers.[16,22–25] Furthermore, it has been shown that retroviral recombination under anti-viral-drug selective pressure can generate viral progeny with enhanced or dual-resistant mutations.[10,11,26] The impact of the RT dipeptide insertion on other biochemical activities, such as the strand transfer activity of HIV-1 RT, remains to be explored.

In this study, we characterized the biochemical recombination capability of two clinical RT variants that have been previously isolated from a single HIV-1 patient before and after HAART, termed pre-drug RT and post-drug RT, respectively: post-drug RT is a dipeptide insertion RT containing a Ser-Gly insertion mutation at positions 69 and 70 of the fingers domain along with a T215Y TAM. Our study reveals that the post-drug RT has elevated strand transfer activity and an altered interaction with templates compared to the pre-drug RT. More importantly, the removal of the dipeptide insertion from the post-drug RT simultaneously inactivates the elevated strand transfer activity and azidothymidine (AZT) resistance, supporting a mechanistic link between strand transfer and the multiple drug resistance of the dipeptide insertion RT containing T215Y.

Results

Characteristics of an NRTI-resistant HIV-1 RT isolate with a dipeptide insertion in the fingers domain

We obtained two HIV-1 RT clinical clones (through a collaboration with Dr. Jaap Goudsmit) that had been previously isolated from a single patient before and after prolonged treatments with multiple NRTIs, termed pre-drug RT and post-drug RT in this study, respectively. The RT genes were sequenced completely. A portion of the polymerase domain sequence alignment is shown in Fig. 1a. The pre-drug RT does not harbor any previously known RT mutations that render viral resistance to currently available NRTIs and NNRTIs, and has a 97% sequence similarity to the RT of the common laboratory strain NL4-3. In contrast, the post-drug RT clone contains a series of RT mutations throughout the fingers, palm, and thumb domains of HIV-1 RT, including a Ser-Gly (SG) insertion between residues 69 and 70 of the fingers domain and a T215Y TAM mutation. Amino acid substitution mutation differences in the post-drug RT compared to the NL4-3 wild-type (WT) and pre-drug RT showed mutations at I329V, T377R, K4T, and I435V in the connection domain and mutations at R461K, P468S, L469I, and K512Q in the RNase H domain. The genome sequence variations among NL4-3 RT, pre-drug RT, and post-drug RT, characterizing all three RT domains, are summarized in Supplementary Fig. 1. While several additional mutations were identified in the post-drug RT compared to the pre-drug RT, none of these mutations is known to confer RT drug resistance. Figure 1a presents specific amino acid differences in the polymerase domain, which show common mutations that generally accompany the SG insertion at the fingers domain, including the T69S and T215Y TAMs known to render viral resistance to multiple NRTIs.[8,17,23] The T215Y mutation is persistently found in zidovudine (AZT)-resistant RT populations and has been shown to enhance primer unblocking in the presence of a dipeptide insertion.[16,19,25]

Next, we confirmed the effect of the SG dipeptide insertion of the post-drug RT on biochemical AZT

(a)

Base	NL4-3	Pre-drug RT	Post-drug RT
38	C	C	S
67	D	D	S
69	T	T	S
-	-	-	**S**
-	-	-	**G**
70	K	K	**A**
102	Q	**K**	**K**
122	K	**E**	K
135	I	I	**T**
162	C	**S**	**S**
196	G	G	**E**
200	T	T	**I**
207	Q	Q	**E**
211	R	R	**K**
214	F	**L**	F
215	T	T	**Y**
245	V	V	**Q**
257	I	I	**L**
272	A	**P**	A
280	C	C	**S**
286	T	T	**A**
288	A	A	**S**
293	V	**I**	V
294	P	P	**Q**

(b)

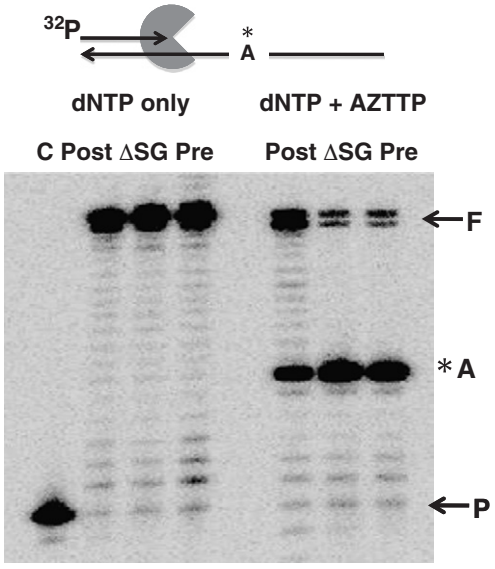

Fig. 1. Sequence comparison of the fingers domain dipeptide insertion HIV-1 RT variants during NRTI therapy and their effects on AZTTP sensitivity. (a) The full-length RT genes isolated from the same individual before NRTI treatment (pre-drug RT) and after NRTI treatment (post-drug RT) were sequenced and compared to WT RT of NL4-3. Only the RT polymerase domain is shown. The shaded boxes are NRTI multiple-drug-resistant mutations. Amino acids in boldface represent mutations that are different from the NL4-3 sequence. (b) AZTTP-terminated primer unblocking. A 5′-end-labeled 20-mer primer annealed to a 38-mer DNA template with only one dTTP/AZTTP incorporation site shown as "*A" was extended by post-drug RT (post), pre-drug RT (pre), and post-drug ΔSG RT (ΔSG). In the absence of AZTTP, the reaction was incubated at 37 °C for 5 min. In the presence of AZTTP, the reaction was incubated at 37 °C for 30 min with all dNTPs (100 μM), except dTTP and dATP. Additional 100 μM dTTP and 3.2 mM ATP were added to the reaction, incubated for an additional 30 min at 37 °C, and terminated.

resistance using 3′-azido-3′-deoxy-thymidine-5′-triphosphate (AZTTP) inhibition assay. For this test, we additionally constructed an SG deletion mutant form of the post-drug RT (post-drug ΔSG RT). We then determined how to set the three proteins to equal polymerase activity using a primer extension reaction with a 5′-end ^{32}P-labeled 23-mer primer annealed to a 38-mer DNA template, carried out at 250 μM dNTPs (Supplementary Fig. 2). As shown in Supplementary Fig. 2, all three RT proteins displayed a similar level of primer extension reaction in 5-min reactions, as estimated by the percentage of the 38-nt-long full-length product ("F").

Next, we repeated the same experiment as the control experiment with a longer incubation time (30 min), which generated a complete extension of the primer to the full-length product in the absence (Fig. 1b, "(–) AZTTP") and in the presence (Fig. 1b, "(+) AZTTP") of 25 mM AZTTP. In this reaction, the template sequence harbors a single TTP incorporation

site, which is also the AZTTP incorporation site ("A" site in Fig. 1b). AZTTP incorporation by RT at this site terminates the primer extension. However, RT proteins carrying AZT resistance will remove the incorporated 3′-azido-3′-deoxythymidine monophosphate (AZTMP) by pyrophosphorolysis excision (or AZTMP unblocking) and continue the primer extension, generating the full-length product. As shown in Fig. 1b, upon the addition of AZTTP to the reaction, the post-drug RT was able to extend past the AZTTP incorporation site ("A" site) and continue primer extension, generating a significant amount of the full-length product. In contrast, the pre-drug RT was unable to overcome the primer block by AZTTP beyond the "A" site, as evident from the little generation of the full-length extension product ("F" in Fig. 1b). This is consistent with previous findings in which RT with dipeptide insertion and T215Y enhanced primer unblocking.[16,22,23,25] Significantly, when the dipeptide insertion was removed from the post-drug RT, the primer unblocking activity diminished to levels similar to the pre-drug RT. This is consistent with previous findings in which RTs with the dipeptide insertion and background T215Y TAM greatly render AZT resistance by enhanced primer unblocking.[22,23] T215Y TAM mutation has been known to aid in positioning the ATP pyrophosphate donor during AZT-mediated excision.[25] However, T215Y mutation alone has greatly diminished primer unblocking abilities due to its inability to synthesize beyond the AZTTP incorporation site upon removal of the SG insertion.

Strand transfer activity of pre-drug and post-drug HIV-1 RT proteins

The structures of HIV-1 RT binary (RT-T/P) and ternary (RT-T/P-dNTP) polymerization complexes showed that the fingers domain of HIV-1 RT where the dipeptide insertion was found directly interacts with the template.[17,27,28] In addition, the stable interaction of HIV-1 RT with the template, which is essential for efficient RNA template cleavage by the RNase H activity of RT, plays a key role in the template-switching (recombination) activity of HIV-1 RT between two homologous RNA strands.[4,29–31] Thus, we hypothesized that the SG dipeptide insertion found in the fingers domain affects the strand transfer activity of HIV-1 RT. To test this hypothesis, we examined the strand transfer activity of the pre-drug RT and the post-drug RT.

Figure 2 is a diagram that depicts the strand transfer system used in our previous study.[29,30] In this system, a 5′-end ^{32}P-labeled 20-nt DNA primer is annealed to an 80 -nt "donor" non-viral RNA sequence template.[26] The acceptor RNA strand is 119 nt long and contains a 64-nt homology region shared with the donor template to allow internal strand transfer events. In addition, the acceptor template has a 19-nt insert (INT. Seq.) near its 5′ end that is not homologous with the donor, as well as an identical 16-nt sequence that is also found at the 5′ end of the donor. The 16-nt at the 5′ end of both the donor and the acceptor are complementary allowing end-transfers with this substrate. However, end-transfer products are not detectable with SDS-PAGE because they were not synthesized over the 19-nt non-homologous insert leaving these products the same length as donor extension products. The primer 3′ terminus has a 3-nt mismatch with the acceptor RNA to prevent the extension of any primer that equilibrates to the acceptor before performing some synthesis on the donor. This system was designed to monitor template switches only between the 64-nt homology regions of the donor and acceptor templates, generating a 119-nt-long transfer product.[26] Thus, strand transfer efficiency can be measured by quantifying the 119-nt-long internal transfer product as a percentage of all products of primer extension.

Strand transfer reactions were carried out as described in Materials and Methods. In making a comparison between RTs, we found it important to perform the assay at equivalent polymerization activities and to compare samples at equivalent times because the transfer efficiency measured *in vitro* rises with both RT concentration and time. First, the total DNA polymerase activity of pre-drug and post-drug RTs was normalized by the quantitation of the amount of the 80-nt fully extended product in the time-course reactions only with the donor template (Fig. 2a). Next, identical donor extension reactions were repeated but in the presence of the acceptor template, with the two RT proteins displaying similar RT activities. As shown in Fig. 2b at the 30-min time point, the post-drug RT yielded more strand transfer products ("TP") than the pre-drug RT. The strand transfer efficiencies of these two RT proteins were determined as previously described and compared at 15-min and 30-min time points. The percentage of transfer products was calculated using the equation $[TP/(TP+F)]$,[31] where TP is the amount of transfer product and F is the amount of full-length extension product only on the donor template. Indeed, as shown in Fig. 2c, the post-drug RT at 30 min showed a 2-fold-higher transfer efficiency than the pre-drug RT. These results indicate that the post-drug RT containing the SG dipeptide insertion, along with T215Y, is more effective at executing a template switch during reverse transcription than the pre-drug RT.

Is enhanced strand transfer a direct result of dipeptide insertion?

Since the post-drug RT that we employed in this study contains the T215Y TAM and the dipeptide insertion, we tested whether the enhanced strand transfer efficiency observed in the post-drug RT

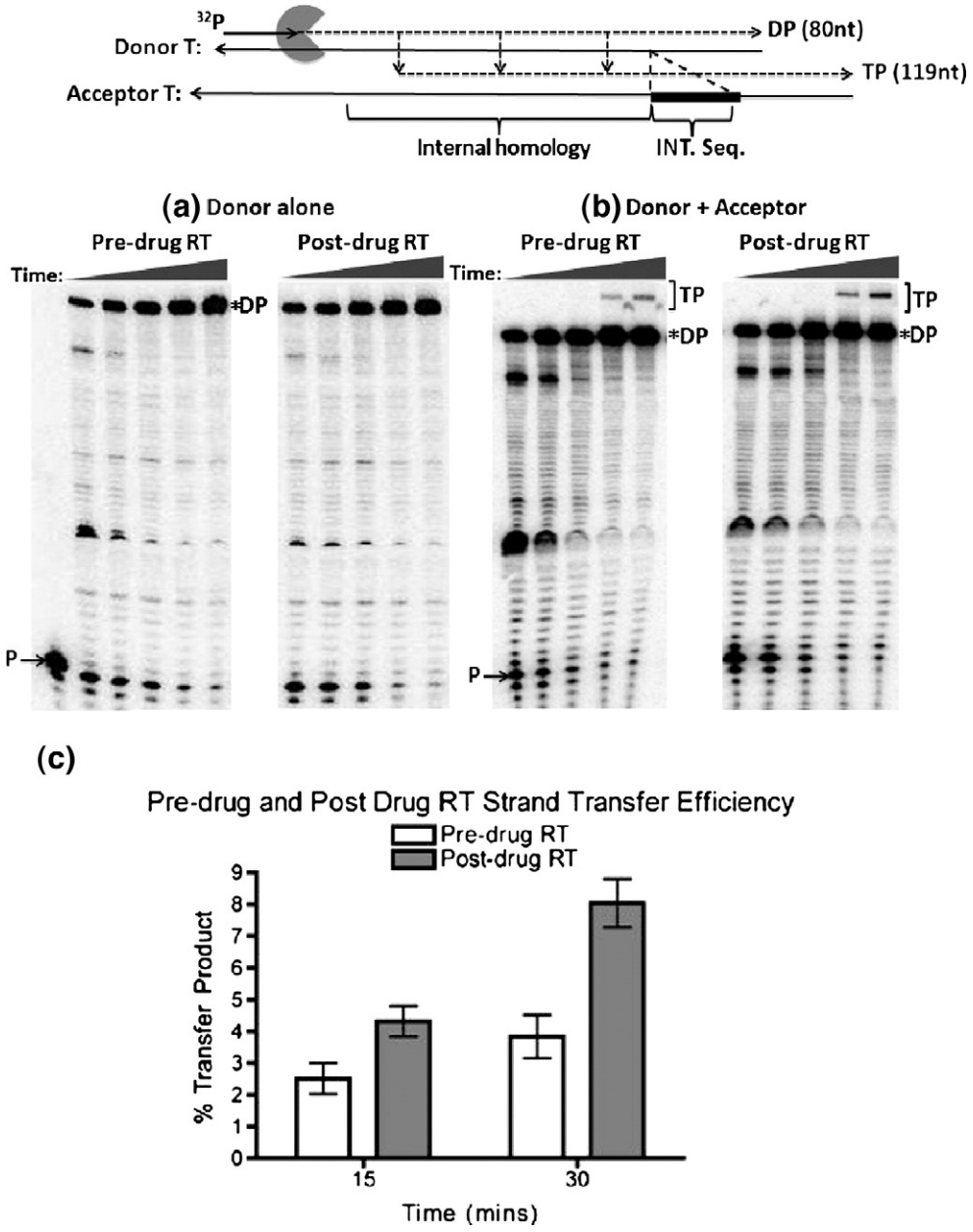

Fig. 2. Strand transfer efficiency of the pre-drug RT and post-drug RT proteins. (a) Diagram for the strand transfer assay substrates. The donor and acceptor RNAs are 80 nt and 119 nt long, respectively. Both templates share a 64-nt homology region for internal strand transfer, with the acceptor template carrying a 19-nt disrupted homology region (INT. Seq.). Primer extension shows similar amounts of pre-drug RT and post-drug RT activities placed into each transfer reaction. P = unextended primer; DP = donor product fully extended at 80 nt. (b) Strand transfer efficiency of the pre-drug and post-drug RT variants. A 5′-end ^{32}P-labeled 20-nt DNA primer is annealed to the 80-nt donor RNA for primer extension, with the addition of the 119-nt acceptor RNA in this time-course assay and with earlier time points showing the RT primer extension activity placed into each reaction (0.5 min, 1 min, 3 min, 15 min, and 30 min). P = unextended primer; DP = donor product fully extended at 80 nt; TP = 119 -nt transfer product. (c) Quantitative analysis of the strand transfer efficiency of the pre-drug and post-drug RT variants at the 15-min and 30-min time points. The experiments were repeated at least in triplicate with $p < 0.05$ at 30-min time points.

(Fig. 3) derives from the dipeptide insertion. For this test, we removed the SG between positions 69 and 70 from the post-drug RT, leaving other RT mutations, including T215Y, unchanged. Using the same template as in Fig. 2, we first normalized the activities of all three RTs (pre-drug RT, post-drug

RT, and post-drug ΔSG RT) in an extension reaction in Supplementary Fig. 3 and quantified them in Fig. 3a. Then, at comparable polymerase activities of the three RT proteins, the strand transfer efficiencies of the three RT proteins were measured as described in Fig. 2. Figure 3b and c shows the strand transfer assay results: indeed, the post-drug RT produced a higher percentage of transfer products at 15 min and 30 min than the pre-drug RT, confirming the data in Fig. 2. Importantly, post-drug ΔSG RT showed reduced strand transfer efficiency compared to the post-drug RT and has a strand transfer efficiency similar to pre-drug RT. To further validate our results with a more biologically relevant form of RT, we utilized a heterodimer pre-drug RT and a post-drug RT for the strand transfer assay. Supplementary Figure 4 shows quantified data of a time-course primer extension assay used for normalizing RT activity. The purpose was to normalize the heterodimer pre-drug RT and post-drug RT activities used in the strand transfer assay. Supplementary Figure 5 shows that the heterodimer post-drug RT contains a higher strand transfer activity than the heterodimer pre-drug RT even when less RT activity was placed into the reaction. The results above support the conclusion that the SG dipeptide insertion is mainly responsible for the elevated strand transfer activity of the post-drug RT. Other mutations specific for the post-drug RT, including T215Y (Fig. 1), do not significantly contribute to the elevated strand transfer efficiency.

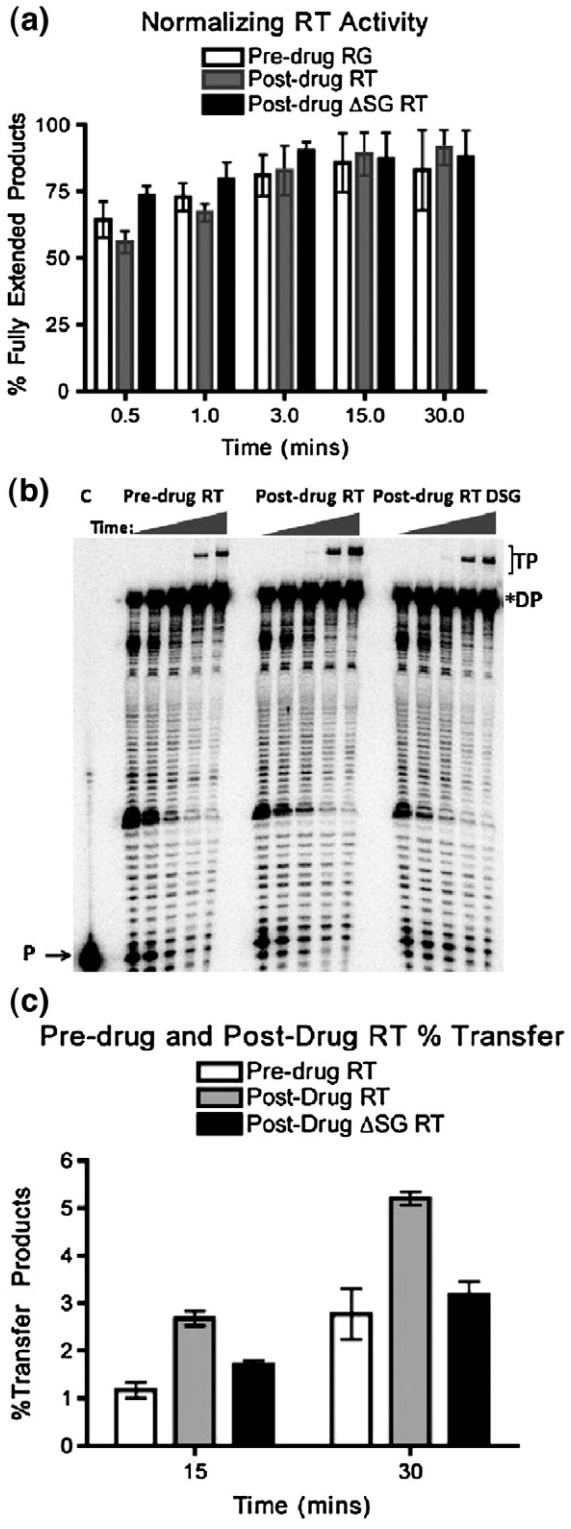

Fig. 3. Strand transfer efficiency of the pre-drug RT, post-drug RT, and post-drug ΔSG RT proteins. (a) The activities of the pre-drug RT, post-drug RT, and post-drug ΔSG RT proteins from (a) were quantified with primer extension assay using the same T/P substrate used in the strand transfer reaction represented in (b). The activities of all three RT proteins were normalized and quantified at each time point for a fully extended 80-nt donor product starting at 0.5 min, 1 min, 3 min, 15 min, and 30 min. The percentage of a fully extended product was calculated with $(F/F+P)\times 100$. Error bars represent results in triplicate. (b) Strand transfer efficiency of pre-drug RT, post-drug RT, and post-drug ΔSG RT. (c) Quantitative analysis of the strand transfer efficiency of the pre-drug RT and post-drug RT variants from (c). Statistical analysis with paired t test resulted in $p<0.05$ at 30 min for the strand transfer efficiency bar graph. P = primers; DP = donor fully extended at 80 nt; TP = 119-nt transfer products.

Confirmation of the elevated strand transfer efficiency of post-drug RT using another strand transfer system

To ensure that the enhanced strand transfer efficiencies that we measured for post-drug RT were not biased because of the specific sequence template employed, we used another strand transfer system previously described:[31] this system employs a 184-nt donor template and a 227-nt acceptor RNA encoding a portion of the HIV Pol gene, as described in the diagram at the top of Fig. 4.[31,32] In this system,

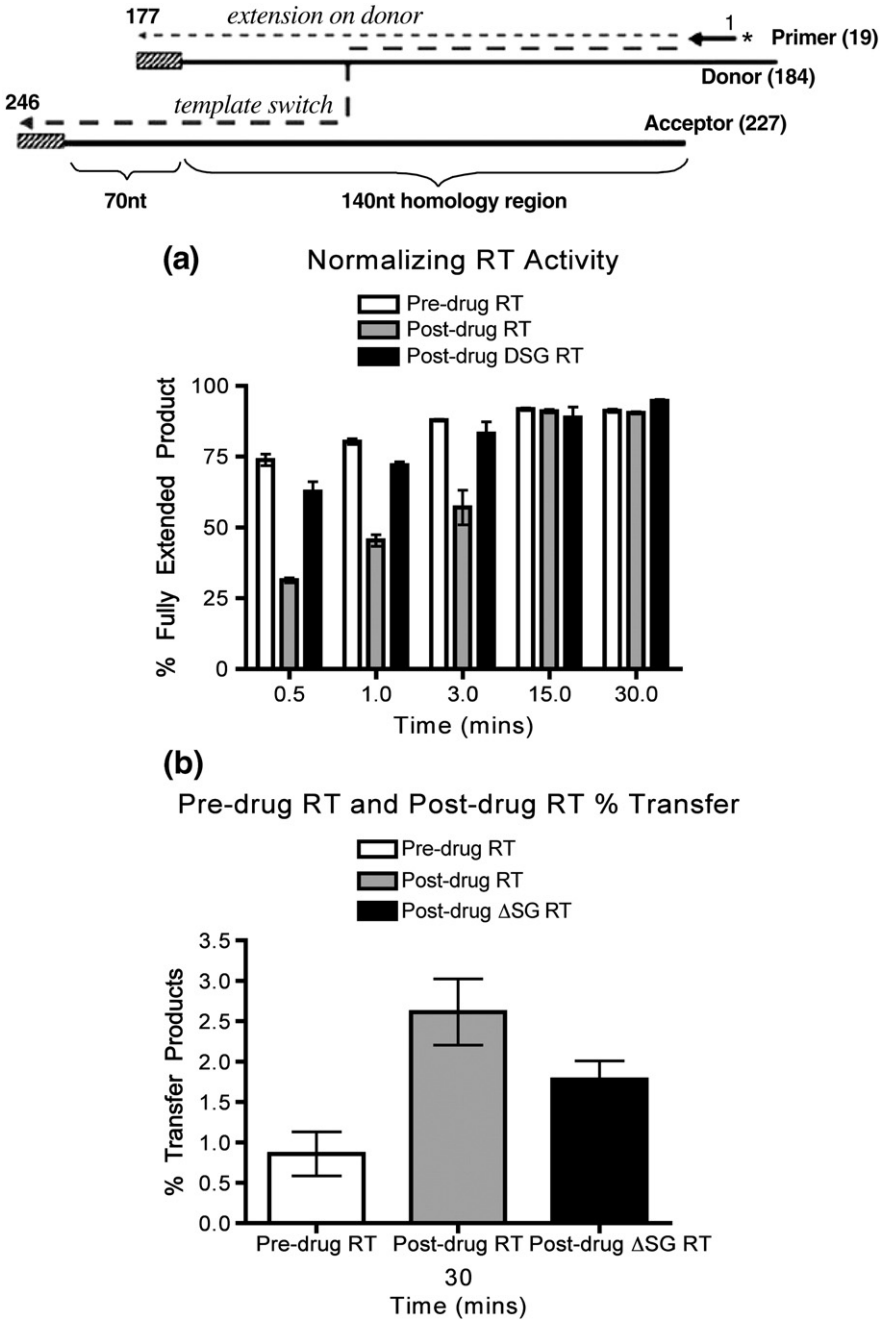

Fig. 4. Strand transfer efficiency of the pre-drug RT, post-drug RT, and post-drug ΔSG RT proteins using a sequence template derived from HIV-1 Pol. (a) Diagram for the strand transfer assay substrates.[31] The donor and acceptor RNAs are 184 nt and 227 nt long, respectively. Both templates share a 140-nt homology region for internal strand transfer, with the donor template carrying a 16-nt disrupted homology (slash box) region to prevent end transfer. The 5′-end ^{32}P-labeled 20 -nt DNA primer is annealed to the donor RNA. Normalized activities of the pre-drug RT, the post-drug RT, and the post-drug RT ΔSG were established through a 184-nt donor extension assay and quantified to ensure that the same amount of RT activities was used for each reaction. (b) Quantitative analysis of the strand transfer efficiency of all three RT variants at the 30-min time point using this strand transfer system. Strand transfer experiments were repeated at least in triplicate.

internal transfer during the donor template replication generates a long product (227 nt), while the donor extension without transfer generates a short product (184 nt). First, RT activities were normalized and quantified in Fig. 4a to ensure that similar amounts of RT activities were placed into each strand

transfer reaction. The transfer assay was then performed with both donor and acceptor RNA templates. As shown in Fig. 4b, the post-drug RT showed the highest strand transfer efficiency at 30 min. These results confirmed that the post-drug RT containing SG has higher strand transfer activity than pre-drug RT and post-drug ΔSG RT, using a second template system.

Processivity of pre-drug RT and post-drug RT

Low processivity has been shown to contribute to elevation of strand transfer efficiency.[33] Although a previous study has shown that HIV-1 RT containing T69S, SG insertion, and K79R did show a slight decrease in processivity compared to WT HIV-1 RT, our base substitution mutations are slightly different from previous work and need to be confirmed.[16] This will deduce whether processivity plays a mechanistic role in the enhanced strand transfer observed for the post-drug RT. The processivity assay was carried out using the 184-nt donor RNA substrate in the presence of a poly(rA)–oligo(dT) trap. Equal pre-drug RT and post-drug RT activities were normalized through a primer extension assay in the absence of the poly(rA)–oligo(dT) trap (Supplementary Fig. 6, lanes 1 and 5, respectively) using the substrate described in Materials and Methods. In the presence of the trap, RT will only be able to undergo one round of primer extension. Once the RT dissociates, it will bind to the excess trap and no longer will be able to reinitiate primer extension. A 1000-fold excess of trap was added to the reaction mix before the addition of RT to produce a trap control, as shown in lanes 3 and 7 of Supplementary Fig. 6. The processivity of the pre-drug RT and the post-drug RT is shown in Supplementary Fig. 6 (lanes 4 and 8, respectively). The substrate was pre-incubated with RT before the initiation of the reaction with dNTP, $MgCl_2$, and trap. The pre-drug RT and the post-drug RT exhibit similar processivities, since both were able to extend the primers to full-length products. Lower processivity is not the mechanism responsible for the enhanced strand transfer seen in the post-drug RT.

Donor template degradation during primer extension

During proviral DNA synthesis, HIV-1 RT degrades the RNA template during and after DNA synthesis.[4,34] RNA template degradation is an essential step for the transfer of the first strong-stop DNA from the 5′ end of the viral genome to the 3′ end of the genome because the first strong-stop DNA must be freed from the RNA template to execute the strand transfer.[4,35] The degradation of donor RNA template is catalyzed by two different types of RNase H activity for RT:[31,34,36,37] RT exhibits RNase H activity while it is polymerizing (called polymerization-dependent RNase H activity), and RT also binds in a 5′ orientation to segments of RNA annealed to DNA, where it can cleave the RNA (called polymerization-independent RNase H activity).[34,38] Thus, to measure the essential determinant of strand transfer efficiency, we analyzed the donor RNA degradation executed by both RNase H DNA polymerization-dependent and polymerization-independent processes.

We tested whether strand transfer activity differences between the pre-drug RT and the post-drug RT were a consequence of differences in RNase H activities. More specifically, we postulated that the post-drug RT degrades the donor template more than the pre-drug RT. To examine the donor template degradation profile comparing these two RT proteins during the strand transfer reaction, we employed the 5′-end ^{32}P-labeled donor 80-nt RNA template, instead of the 20-mer primer, to monitor donor RNA degradation during the strand transfer assay. The total RT polymerization activity of the two RT proteins used in this reaction was the same as that used for the transfer reaction in Fig. 3. Since the reactions included dNTPs, the template degradation should have been catalyzed by both DNA polymerization-dependent and polymerization-independent RNase H activities of RT. As shown in Fig. 5, the post-drug RT had less template degradation through the initial three time points but showed no difference in template degradation through the last two time points when compared to the pre-drug RT. The same experiment was repeated with the post-drug ΔSG RT, and results showed no major differences in template degradation from the pre-drug RT and the post-drug RT. This shows that the elevated strand transfer events seen with the post-drug RT do not appear to be a consequence of the overall donor template degradation, which is catalyzed by both polymerization-dependent and polymerization-independent RNase H activities.

Assessing the individual polymerization-dependent and polymerization-independent RNase H activities of pre-drug and post-drug RT proteins

Since the donor template degradation described in Fig. 5 was catalyzed by both polymerization-dependent and polymerization-independent RNase H activities of RT, we examined the polymerization-dependent RNase H activities of the pre-drug, post-drug, and post-drug ΔSG RTs. For this assay, a 32-nt-long DNA primer was annealed to a 5′-end ^{32}P-labeled 38-nt RNA template, and this RNA/DNA hybrid substrate (see diagram in Fig. 6) was incubated separately with the three RT

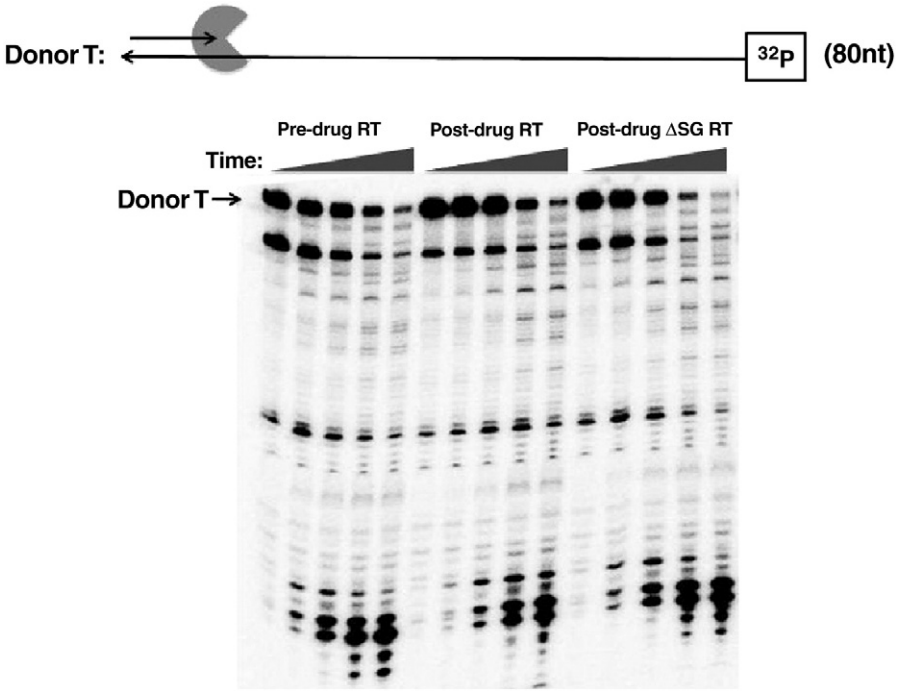

Fig. 5. Donor template degradation of pre-drug RT, post-drug RT, and post-drug ΔSG RT. A ^{32}P-labeled 80-nt donor RNA template was annealed to cold 20-nt DNA primers at a 1:2 ratio. Pre-drug RT, post-drug RT, and post-drug ΔSG RT were pre-incubated with the T/P complex for 3 min before the addition of 6 mM $MgCl_2$/5 μM dNTP for initiation of the reaction. Reactions were quenched with EDTA in the following time-course assay at 0.5 min, 1 min, 3 min, 15 min, and 30 min. Donor T: ^{32}P-labeled 80-nt donor RNA template. The RT activities were similar to those shown in Fig. 3.

proteins, showing an equal RNA-dependent DNA polymerase activity in the absence of dNTPs. As shown in Fig. 6, the post-drug RT showed faster degradation of the 38-nt full-length RNA substrate than the pre-drug RT and the post-drug ΔSG RT. In this polymerization-dependent RNase H assay, RT molecules, which are engaged in DNA synthesis, execute the two sequential cleavage events: (1) 1° cleavage of the donor RNA template, generating 25-nt-long products, and (2) 2° cleavage for further degradation of the 1° cleavage product, generating 13-nt-long products.[31] Indeed, as shown in the quantified time-course degradation profile (Fig. 6b), the post-drug RT protein displayed a faster accumulation of both 1° and 2° cleavage products. These data suggest that the post-drug RT polymerization-dependent RNase H activity is faster, contributing to its higher strand transfer activity compared to the pre-drug RT and the post-drug ΔSG RT. Importantly, the lower RNase H activity of the post-drug ΔSG RT suggests that the dipeptide insertion is responsible for not only the elevated strand transfer activity but also the enhanced polymerization-dependent RNase H activity of the post-drug RT. Next, we examined the polymerization-independent RNase H activities of the pre-drug, post-drug, and post-drug ΔSG RTs as described in Materials and Methods (Supplementary Fig. 7). Interestingly, we found that the post-drug RT actually has reduced polymerization-independent RNase H activity compared to the pre-drug RT and the post-drug ΔSG RT. This suggests that the delayed donor template degradation by the post-drug RT (Fig. 5) could be due to its reduced polymerization-independent RNase H activity, and also that polymerization-independent RNase H activity is not the mechanism involved in the elevated strand transfer efficiency of the post-drug RT.

Determining the template/primer binding affinity (K_d), on-rate (k_{on}), and off-rate (k_{off}) of pre-drug RT, post-drug RT, and post-drug ΔSG RT

To complete the mechanistic investigation of the elevation of the strand transfer activity of post-drug RT, we determined the K_d value of HIV-1 RT. This parameter numerically represents steady-state equilibrium events between the rate of RT initial binding to template/primer (T/P) (k_{on}) and the rate of RT release from T/P (k_{off}). Since the fingers domain of HIV-1 RT harboring the dipeptide insertion directly interacts with the template, we reasoned that the higher strand transfer activity and the elevated polymerization-dependent RNase H activity of the post-drug RT may result from an altered binding

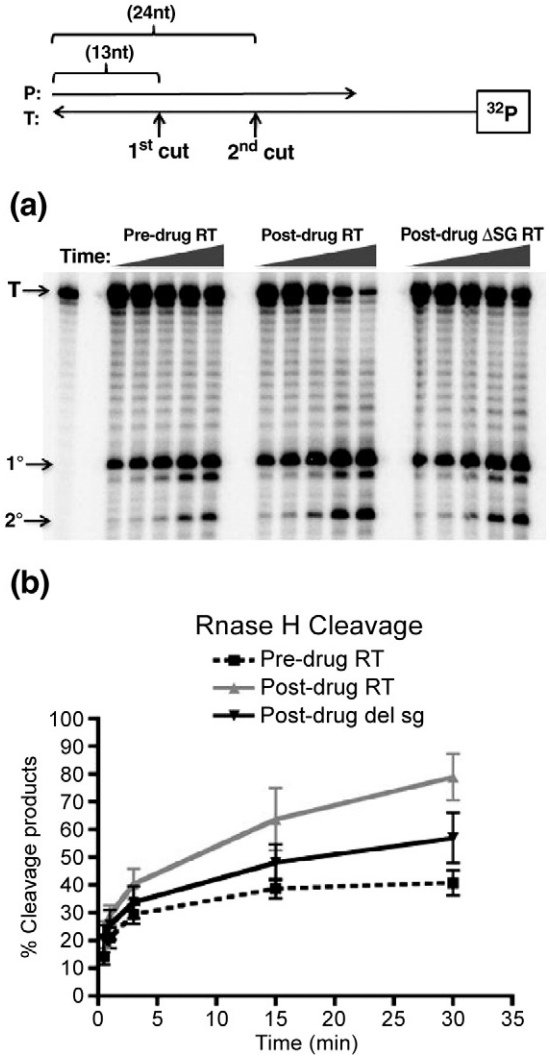

Fig. 6. RNase H assay consisted of a 5′-end ^{32}P-labeled 38-mer RNA annealed to a 32-nt unlabeled DNA primer. (a) The same amount of RT activities used in Fig. 3 was used for this assay. The reaction was carried out in a time-course assay (0.5 min, 1 min, 3 min, 15 min, and 30 min) in the absence of dNTP and quenched with the addition of EDTA. RNase H cleavages yielded a 24-nt primary-cut product and a 13-nt secondary-cut product. (b) Quantification of RNase H 5′-end ^{32}P-labeled 38-mer RNA degradation from (a) shows the percentage of degraded RNA over time. Percent degraded RNA was calculated based on the amount of (saturated volume from 1°+2° cleavages)/(saturated volume from 1°+2° cleavages+uncut)×100.

affinity of the RT for the T/P complex. It is possible that the increased T/P binding affinity of the post-drug RT may be due to either a faster initial T/P binding rate or a slower releasing rate from T/P.

First, we measured the binding affinity (K_d) of the pre-drug RT and post-drug RT proteins for T/P (a 19-nt primer annealed to a 184-nt RNA template) using a double-filter binding blot assay, which uses both protein and nucleic acid binding filters (see Materials and Methods), and the percentages of bound DNA *versus* RT concentrations were plotted on a sigmoidal binding curve.[39] As summarized and shown in Table 1, the post-drug RT displayed a lower K_d (equilibrium binding constant) value than the pre-drug RT and the post-drug ΔSG RT (pre-drug RT $K_d = 5.9\times10^{-7}$ M; post-drug RT $K_d = 7.8\times10^{-8}$ M; post-drug ΔSG RT $K_d = 1.7\times10^{-7}$ M). From these data, we conclude that the post-drug RT has seven times higher binding affinity for T/P than the pre-drug RT and three times higher binding affinity than the post-drug ΔSG RT. Second, we measured the k_{off} of the RTs using the RT off-rate assay previously reported.[33] Using a primer extension assay with the addition of a >1000-fold molar excess of the poly(rA)–oligo(dT) trap, we determined the amount of RT bound to the template based on primer extension. Since RT dissociation from the substrate is slower than dNTP incorporation, the amount of primer extension was representative of RT bound to the substrate.[33,40] The trap was incubated at increasing time points, with RT pre-bound to T/P (2 nM). In this system, RT molecules that dissociated from T/P will be captured by the poly(rA)–oligo(dT) trap (8000 nM) and are no longer able to extend the primer in the presence of dNTP and $MgCl_2$. Therefore, this experiment measured a single round of primer extension. Table 1 presents a summary of our k_{off} data extrapolated from the exponential decay curve based on the equation $Y = e^{-k_{off}(t)}$, where Y is the relative rate of incorporation and t is time.[33] From these exponential decay equations, we calculated the k_{off} values of all three RTs as follows: pre-drug RT $k_{off} = 6.1\times10^{-4}$ s^{-1}; post-drug RT $k_{off} = 3.1\times10^{-4}$ s^{-1}; post-drug ΔSG RT $k_{off} = 2.6\times10^{-4}$ s^{-1}. Basically, the k_{off} difference between the two RT proteins was only two fold. Finally, using the K_d values and the k_{off} values,

Table 1. The K_d, k_{off}, and k_{on} values of pre-drug RT and post-drug RT

	K_d[a] (M)	k_{off}[b] (s^{-1})	k_{on}[c] (M^{-1} s^{-1})
Pre-drug RT	5.9×10^{-7} ±0.0616	6.1×10^{-4} ±0.0105	1.9×10^{4}
Post-drug RT	7.8×10^{-8} ±0.2761	3.1×10^{-4} ±0.0167	3.5×10^{5}
Post-drug ΔSG RT	1.7×10^{-7} ±0.2560	2.6×10^{-4} ±0.0217	1.5×10^{5}

[a] DNA binding study summarized. The K_d of each RT isolate was extrapolated from a sigmoidal binding curve.
[b] k_{off} was calculated from the exponential decay equation $Y = e^{-k_{off}(t)}$, where Y is the relative rate of incorporation and t is time. Each data point represents the value from three independent experiments, with standard error.
[c] Quantification of the percent bound DNA of all three RT protein isolates. The k_{on} values of the three RTs were calculated using the equation $K_d = k_{off}/k_{on}$.

which were experimentally measured, we are able to calculate the on-rate (k_{on}) of the RTs using the equation: $K_d = k_{off}/k_{on}$. The calculated k_{on} values of the three RT proteins were roughly as follows: pre-drug $k_{on} = 1.9 \times 10^4$ M^{-1} s^{-1}; post-drug RT $k_{on} = 3.5 \times 10^5$ M^{-1} s^{-1}; post-drug ΔSG RT $k_{on} = 1.5 \times 10^5$ M^{-1} s^{-1} (Table 1). These k_{on} values data imply that the post-drug RT is able to associate with its T/P substrate 18 times faster than the pre-drug RT and 8 times faster than the post-drug ΔSG RT. Mechanistically, this may contribute to the tight binding affinity of T/P.

Discussion

Interstrand homologous recombination of HIV-1 occurs mainly during minus-strand proviral DNA synthesis. Recombination enhances viral diversity and facilitates HIV-1 escape from anti-viral selective pressures, including HAART.[5,9,41] The dipeptide fingers domain insertion is positioned at the end of the HIV-1 RT fingers domain and in the cleft where the T/P hybrid binds, but far from the polymerase active site.[27,42] Interestingly, although they are located outside of the polymerase active site, these mutations are associated with viral resistance to multiple NRTIs such as AZT, which bind to the polymerase active site.[8,18]

HIV-1 RT interactions with the double-stranded region of the template annealed to the primer were extensively studied.[43] However, RT interactions with the single-stranded portion of the template are less well understood. Moreover, the structure of the tertiary complex of HIV-1 RT and of a template with an extended single-stranded portion is not available. Positioning of the single-stranded part of the template at the cleft near the tip of the fingers domain has been predicted but not proven.

Significantly, the fingers domain of HIV-1 RT undergoes a large conformational change during T/P binding (RT-T/P binary complex formation),[27] and it is highly likely that the β3–β4 loop at the tip of the fingers domain is structurally dynamic during DNA synthesis. The β3–β4 loop is likely the section of the replicating RT molecule that first contacts RNA template secondary structures. It has been shown that stable local structures of the RNA template mechanistically induce RT pausing.[44] Pausing during synthesis in turn facilitates RNA template degradation by the RNase H activity of RT, which is an essential step for strand transfer.[29,30] Thus, we hypothesized that the dipeptide insertion in HIV-1 RT, which lies at the tip of the fingers domain, may alter RT–RNA template interaction and, thus, the strand transfer efficiency of HIV-1 RT.

The biochemical data in this report demonstrate that the SG insertion RT at the β3–β4 loop has altered RNA binding kinetics of HIV-1 RT, which also is likely to relate to the enhancement of the strand transfer activity. More importantly, the post-drug RT displayed a faster initial binding rate (k_{on}) than the pre-drug RT, leading to seven times higher template binding affinity (K_d) than the pre-drug RT and three times higher binding affinity than the post-drug ΔSG RT. Thus, these biochemical data support the idea that the SG fingers domain insertion elevates the transfer activity presumably by an enhanced interaction with the RNA templates.

An enhanced binding of post-drug RT to T/P could also be related to a mechanism that had been previously proposed for AZT-resistant mutations found at the connection domain of HIV-1 RT: connection mutations stabilize the RT–template complex, yielding more time for the bound RT molecule to remove the incorporated AZTMP at the 3′ end of the primer.[45] Similarly, the dipeptide insertion may also confer AZT resistance by enhancing binding affinity, which lengthens the time span for HIV-1 RT to remain bound to the 3′ end of the primer for pyrophosphorolysis of AZTMP. We also envision that the increased frequency of the binding of post-drug RTs to T/P can increase the degradation capability of the RNA template by the RT polymerization-dependent and polymerization-independent RNase H activities, which in turn would enhance the strand transfer activity. Importantly, our data demonstrate that the removal of the dipeptide insertion from the mutant concomitantly induces the loss of both AZTMP pyrophosphorolysis and elevated strand transfer. This supports the idea that AZT resistance and elevated strand transfer share a common mechanism—enhanced interaction with the RNA template.

It is well established that the efficient RNA template degradation by RNase H increases the strand transfer of RT.[29,30,36,37,42,46] As shown in Fig. 6b, the pre-drug RT showed a higher polymerization-dependent RNase H activity and a faster rate of binding (k_{on}) to the template (Table 1), compared to the pre-drug RT. These two biochemical alterations by the dipeptide insertion can mechanistically contribute to the enhanced strand transfer efficiency of the post-drug RT: the post-drug RT creates a 1° cleavage of the donor template more efficiently, followed by a faster 2° cleavage of the donor template, compared to the pre-drug RT. These elevated 1° and 2° cleavages during DNA synthesis will generate more gaps, which serve as evasion sites for the acceptor RNA template during template switch and ultimately increase strand transfer activity. Importantly, the fast binding rate (k_{on}) of the post-drug RT can facilitate the 2° cleavage of the donor template, which likely requires the rebinding of RT after the 1° cleavage. Importantly, the overall delayed template degradation of the post-drug RT (Fig. 5) is the result of both polymerization-

dependent and polymerization-independent RNase H activities. As shown in Supplementary Fig. 7, the post-drug RT actually has reduced polymerization-independent RNase H activity compared to the pre-drug RT. Thus, these two sets of data suggest that the polymerization-independent RNase H activity that could be responsible for the delayed template degradation is not mechanistically involved in the elevated strand transfer activity of the post-drug RT. Instead, the polymerization-dependent RNase H activity, which creates the invasion sites for the acceptor during DNA synthesis, is more likely the mechanistic reason for the elevated strand transfer activity of the post-drug RT.

In summary, the multiple-drug-resistant post-drug RT displayed altered biochemical behaviors, including elevated strand transfer activity, increased polymerization-dependent RNase H activity, and tighter binding affinity for the T/P substrate. We believe that with these simultaneous mechanistic changes made by the dipeptide insertion RT, a follow-up virological experiment to test the actual impact of the post-drug RT mutations on the recombination efficiency of the viruses should be conducted in the future.

Materials and Methods

HIV-1 RT proteins

Two HIV-1 RT clinical clones named pre-drug RT and post-drug RT were kindly provided by Dr. Jaap Goudsmit (Amsterdam Medical Center, Netherlands). These RT genes were cloned into an *Escherichia coli* overexpression plasmid (pHis) and encode a protein with a fused 6-histidine tag at its N-terminal end used for protein purification of homodimer RTs. The clones were transformed into BL-21-competent *E. coli* for protein expression and purified through a nickel column (Novagen). Protein purification methods were performed in accordance with Operario *et al.*[31] The post-drug RT with the ΔSG dipeptide insert was generated using a QuikChange mutagenesis kit (Stratagene), with the post-drug RT clones as template. The primers designed to introduce the SG dipeptide deletion were deleted SG forward primer GAAGAAAAGCAGTAGCGCTTGGAGAAAAT-TAGTAGATTTC and reverse primer GAAATCTAC-TAATTTTCTCCAAGCGCTACTGCTTTTCTTC. The post-drug ΔSG RT clone was sequenced, and all protein purification methods were the same as described above. Heterodimer HIV-1 RT was prepared by cloning the pre-drug or post-drug RT p66 subunit into a pet28a expression plasmid containing a kanamycin selection marker. The p51 subunit derived from HIV-1 RT HXB2 strain was cloned into a pCDF plasmid containing a spectinomycin antibiotic selection marker and a fused 6-histidine tag at its N-terminus. The clones were transformed into BL-21-competent *E. coli* for protein expression, selecting for both antibiotics marker and purified through a nickel column (Novagen).

Generation of RNA templates

RNA templates were generated as described previously.[29,30] Briefly, PCR product was generated using primers PCIS5 and PCIS6 and the pD0 plasmid as template. The PCR product was then purified by agarose gel electrophoresis and a QIAquick gel extraction kit (Qiagen). The T7 RNA polymerase MEGAshortscript kit (Ambion) was implemented for the synthesis of 80-nt donor RNA using the purified PCR product as template and the primer PCIS 14 (TGGTAAACATTCTTGAGTGC). The 119-nt acceptor RNA template was generated from the T7 RNA polymerase MEGAshortscript kit (Ambion) using the previously described plasmid pAM_2.[30] The 184-nt donor and the 227-nt acceptor substrates encode a portion of the HIV-1 Pol gene sequence and were generated as previously described.[31,32]

AZTTP-terminated primer unblocking

A 5′-end-labeled 20-nt primer was annealed to a 38-nt DNA template that had only one dATP downstream of the primer 3′ terminus where a thymidine triphosphate (dTTP) or AZTTP could be incorporated (Fig. 1b, arrow). Primer extension by pre-drug or post-drug RT was performed in the absence or in the presence of 25 μM AZTTP. Synthesis reactions in the absence of AZTTP were carried out at 37 °C for 5 min. In the presence of AZTTP, reactions were incubated at 37 °C for 30 min with all dGTP and dCTP (100 μM). Then 100 μM dTTP and 3.2 mM ATP were added, and the reaction was incubated for an additional 30 min at 37 °C . All reactions were terminated with the addition of 40 mM ethylenediaminetetraacetic acid (EDTA) and 99% formamide.[22]

Strand transfer assay

A 5′-end ^{32}P-radiolabeled 20-nt DNA primer (0.64 nM) was annealed to an 80-nt donor RNA template (4 nM) in RT reaction buffer [50 mM Tris (pH 8), 50 mM KCl, 1 mM DTT, and 1 mM EDTA] at 95 °C for 5 min and slowly cooled to room temperature. RT was incubated with the substrate for 3 min before the reaction was started with the addition of $MgCl_2$ (6 mM), dNTP (50 μM), and 119-nt acceptor RNA template (8 nM). All reactions were performed in a 37. 5-μL master mix volume at 37 °C . Reactions were terminated at various time points by transferring an aliquot of 6.25 μL from the master mix volume into 6.25 μL of 40 mM EDTA and 99% formamide. The second substrate used for this study was a 19-nt 5′-end ^{32}P-radiolabeled DNA primer annealed to a 184-nt RNA template. The acceptor template was a 227-nt RNA template. Both the 184-nt donor and the 227-nt acceptor RNA templates encode a portion of the HIV-1 Pol gene. The exact experimental conditions as described above were applied to this set of substrate. Reaction products were resolved in a 10% polyacrylamide–urea denaturing gel and scanned on a PhosphoImager (Bio-Rad). Percent transfer was calculated [(transfer product/first time-point extension + transfer product) × 100%] based on saturation volume quantified by Quantity One software. Background saturation volume was subtracted from all quantifications.[26,31] The primer extension assay methodology was performed exactly as the strand transfer assay

described above, except that initiation of the reaction did not include the acceptor RNA.

Donor degradation assay

The same 80-nt donor RNA template (50 nM) used for the strand transfer assay was 5′-end-radiolabeled with ^{32}P and annealed with the unlabeled 20-nt DNA primer (100 nM) in RT reaction buffer by heating at 95 °C for 5 min and slowly cooled to room temperature. All reactions were carried out with the same procedures as in the strand transfer assay, except that the initiation of the reaction was performed with $MgCl_2$ (6 mM) and dNTPs (5 μM).

RNase H assay

A 38-nt RNA template (8 nM) was 5′-end ^{32}P-radiolabeled and annealed to a 32-nt DNA primer (32 nM) to measure polymerization-dependent RNase H activity. A 38-nt RNA template (8 nM) was 5′-end ^{32}P-radiolabeled and annealed to a 53-nt DNA primer (32 nM) to measure polymerization-independent RNase H activity. Both polymerization-dependent and polymerization-independent RNase H activity reaction conditions and time points were the same as in the strand transfer assay, except that the initiation of the reaction was performed with only $MgCl_2$ (6 mM). The products were fractionated on a 14% polyacrylamide–urea denaturing gel and analyzed with the same equipment and methods described previously.[31]

Processivity assay

A 19-nt 5′-end ^{32}P-radiolabeled DNA primer was annealed a 184-nt RNA template previously described in the strand transfer experiment as the HIV Pol template at a ratio of 2:1 (8 nM:4 nM final concentration). RT with equal activity was pre-bound to the substrate for 3 min at 37 °C in RT reaction buffer [50 mM Tris (pH 8), 50 mM KCl, 1 mM DTT, and 1 mM EDTA]. The reaction was initiated with the addition of $MgCl_2$ (6 mM), dNTP (25 μM), and a 1000-fold excess of poly(rA)–oligo(dT) trap (IDT) (annealed at a 1:2 ratio, respectively) over the substrate concentration. The final reaction mixture volume was 12.5 μL. The primer extension assay was incubated for 5 min at 37 °C before quenching with 12.5 μL of 40 mM EDTA and 99% formamide. The products were fractionated on a 10% polyacrylamide–urea denaturing gel.[33]

k_{off} measurements (dissociation rate constant)

The 19-nt 5′-end ^{32}P-radiolabeled DNA primer was annealed with the 184-nt RNA template at a 2:1 ratio. RT was pre-bound to the template in the presence of a 1000-fold excess of poly(rA)–oligo(dT) (IDT) annealed at a 1:2 ratio, respectively, and incubated at increasing time points with the reaction mixture before the addition of $MgCl_2$ (6 mM) and dNTP (50 μM). RT that fell off the labeled substrate will bind to the poly(rA)–oligo(dT) trap. RT that remains bound to the labeled substrate after the addition of $MgCl_2$ and dNTP was quantitated by primer extension. The final volume of the reaction mixture containing 50 mM Tris (pH 8), 50 mM KCl, 1 mM DTT, and 1 mM EDTA was 12.5 μL. Reaction products were resolved on a 10% polyacrylamide–urea denaturing gel and scanned with a Bio-Rad PhosphorImager. The relative incorporation values were calculated with the equation: relative incorporation = [(extended product/first time-point extension at 10 s) × 100%]. The saturation volumes used in the above equation to determine relative incorporation were obtained by an analysis of scanned gel images using Quantity One software. All values were normalized with subtracted background values. The dissociation rate was calculated based on an exponential decay graph in which a curve of total relative incorporation *versus* time was fitted to an exponential decay equation: $Y = e^{-k_{off}(t)}$.[33]

K_d measurements (equilibrium dissociation constant)

The double-filter blot assay uses a nitrocellulose membrane that binds RT proteins and a nucleic acid binding nylon membrane (Biodyne Nylon Membrane; VWR). The nylon membrane was washed for 10 min with 0.1 M EDTA and underwent three 10-min washes in 1 M NaCl, followed by a quick wash in 0.5 M NaOH then dH_2O. The nitrocellulose membrane was washed for 10 min with 0.4 M KOH at room temperature and then washed with dH_2O. The membrane was then soaked in 1× dialysis buffer at 4 °C for 1 h before being placed on top of the nylon membrane to create the double-filter blot. The 19-nt DNA primer was 5′-end ^{32}P-radiolabeled and annealed to the 184-nt RNA template used in the strand transfer assay mentioned above using the same substrate described in the k_{off} experiment. The radiolabeled hot primers (8 nM) and non-radiolabeled cold primers (42 nM) were mixed with the RNA template during annealing. The primer concentration/template concentration ratio for annealing was 1:6, respectively. The premixed solutions had a fixed T/P concentration containing increasing concentrations of the RT proteins for each reaction. Each DNA binding reaction was carried out at 37 °C for 3 min before the reactions were terminated by being vacuumed through the double-membrane filters. The RT that is bound to T/P will bind to the nitrocellulose membrane, while T/P substrates without bound proteins will pass through the nitrocellulose membrane and bind to the nylon membrane. The blot was washed with 100 μL of 1× dialysis buffer. The reactions were carried out in the absence of $MgCl_2$ and dNTP. The blots were exposed with a phosphor screen for 20 min and quantified using a PhosphorImager (Bio-Rad). The percentage of RT proteins bound to DNA was quantified based on saturation volume (protein blot/protein blot + DNA blot) × 100%, all subject to subtracted background values) using Quantity One software.[47] K_d was extrapolated from a sigmoidal binding curve.

Acknowledgements

This study was supported by National Institutes of Health grants AI049781 (B.K.) and GM049573 (R.A.B.).

Supplementary Data

Supplementary data associated with this article can be found, in the online version, at doi:10.1016/j.jmb.2011.11.014

References

1. Volberding, P. A. & Deeks, S. G. (2010). Antiretroviral therapy and management of HIV infection. *Lancet*, **376**, 49–62.
2. Preston, B. D., Poiesz, B. J. & Loeb, L. A. (1988). Fidelity of HIV-1 reverse transcriptase. *Science*, **242**, 1168–1171.
3. Mansky, L. M. & Temin, H. M. (1995). Lower *in vivo* mutation rate of human immunodeficiency virus type 1 than that predicted from the fidelity of purified reverse transcriptase. *J. Virol.* **69**, 5087–5094.
4. Basu, V. P., Song, M., Gao, L., Rigby, S. T., Hanson, M. N. & Bambara, R. A. (2008). Strand transfer events during HIV-1 reverse transcription. *Virus Res.* **134**, 19–38.
5. Onafuwa-Nuga, A. & Telesnitsky, A. (2009). The remarkable frequency of human immunodeficiency virus type 1 genetic recombination. *Microbiol. Mol. Biol. Rev.* **73**, 451–480; Table of Contents.
6. Shriner, D., Rodrigo, A. G., Nickle, D. C. & Mullins, J. I. (2004). Pervasive genomic recombination of HIV-1 *in vivo*. *Genetics*, **167**, 1573–1583.
7. Roberts, J. D., Bebenek, K. & Kunkel, T. A. (1988). The accuracy of reverse transcriptase from HIV-1. *Science*, **242**, 1171–1173.
8. Tamalet, C., Yahi, N., Tourres, C., Colson, P., Quinson, A. M., Poizot-Martin, I. *et al.* (2000). Multidrug resistance genotypes (insertions in the beta3–beta4 finger subdomain and MDR mutations) of HIV-1 reverse transcriptase from extensively treated patients: incidence and association with other resistance mutations. *Virology*, **270**, 310–316.
9. Carvajal-Rodriguez, A., Crandall, K. A. & Posada, D. (2007). Recombination favors the evolution of drug resistance in HIV-1 during antiretroviral therapy. *Infect. Genet. Evol.* **7**, 476–483.
10. Kellam, P. & Larder, B. A. (1995). Retroviral recombination can lead to linkage of reverse transcriptase mutations that confer increased zidovudine resistance. *J. Virol.* **69**, 669–674.
11. Moutouh, L., Corbeil, J. & Richman, D. D. (1996). Recombination leads to the rapid emergence of HIV-1 dually resistant mutants under selective drug pressure. *Proc. Natl Acad. Sci. USA*, **93**, 6106–6111.
12. Belec, L., Piketty, C., Si-Mohamed, A., Goujon, C., Hallouin, M. C., Cotigny, S. *et al.* (2000). High levels of drug-resistant human immunodeficiency virus variants in patients exhibiting increasing $CD4^+$ T cell counts despite virologic failure of protease inhibitor-containing antiretroviral combination therapy. *J. Infect. Dis.* **181**, 1808–1812.
13. Shafer, R. W. (2002). Genotypic testing for human immunodeficiency virus type 1 drug resistance. *Clin. Microbiol. Rev.* **15**, 247–277.
14. Eggink, D., Huigen, M. C., Boucher, C. A., Gotte, M. & Nijhuis, M. (2007). Insertions in the beta3–beta4 loop of reverse transcriptase of human immunodeficiency virus type 1 and their mechanism of action, influence on drug susceptibility and viral replication capacity. *Antiviral Res.* **75**, 93–103.
15. Imamichi, T., Murphy, M. A., Imamichi, H. & Lane, H. C. (2001). Amino acid deletion at codon 67 and Thr-to-Gly change at codon 69 of human immunodeficiency virus type 1 reverse transcriptase confer novel drug resistance profiles. *J. Virol.* **75**, 3988–3992.
16. Boyer, P. L., Sarafianos, S. G., Arnold, E. & Hughes, S. H. (2002). Nucleoside analog resistance caused by insertions in the fingers of human immunodeficiency virus type 1 reverse transcriptase involves ATP-mediated excision. *J. Virol.* **76**, 9143–9151.
17. Curr, K., Tripathi, S., Lennerstrand, J., Larder, B. A. & Prasad, V. R. (2006). Influence of naturally occurring insertions in the fingers subdomain of human immunodeficiency virus type 1 reverse transcriptase on polymerase fidelity and mutation frequencies *in vitro*. *J. Gen. Virol.* **87**, 419–428.
18. Larder, B. A., Bloor, S., Kemp, S. D., Hertogs, K., Desmet, R. L., Miller, V. *et al.* (1999). A family of insertion mutations between codons 67 and 70 of human immunodeficiency virus type 1 reverse transcriptase confer multinucleoside analog resistance. *Antimicrob. Agents Chemother.* **43**, 1961–1967.
19. Cases-Gonzalez, C. E., Franco, S., Martinez, M. A. & Menendez-Arias, L. (2007). Mutational patterns associated with the 69 insertion complex in multi-drug-resistant HIV-1 reverse transcriptase that confer increased excision activity and high-level resistance to zidovudine. *J. Mol. Biol.* **365**, 298–309.
20. Winters, M. A., Coolley, K. L., Girard, Y. A., Levee, D. J., Hamdan, H., Shafer, R. W. *et al.* (1998). A 6-basepair insert in the reverse transcriptase gene of human immunodeficiency virus type 1 confers resistance to multiple nucleoside inhibitors. *J. Clin. Invest.* **102**, 1769–1775.
21. De Antoni, A., Foli, A., Lisziewicz, J. & Lori, F. (1997). Mutations in the pol gene of human immunodeficiency virus type 1 in infected patients receiving didanosine and hydroxyurea combination therapy. *J. Infect. Dis.* **176**, 899–903.
22. Mas, A., Parera, M., Briones, C., Soriano, V., Martinez, M. A., Domingo, E. & Menendez-Arias, L. (2000). Role of a dipeptide insertion between codons 69 and 70 of HIV-1 reverse transcriptase in the mechanism of AZT resistance. *EMBO J.* **19**, 5752–5761.
23. Meyer, P. R., Lennerstrand, J., Matsuura, S. E., Larder, B. A. & Scott, W. A. (2003). Effects of dipeptide insertions between codons 69 and 70 of human immunodeficiency virus type 1 reverse transcriptase on primer unblocking, deoxynucleoside triphosphate inhibition, and DNA chain elongation. *J. Virol.* **77**, 3871–3877.
24. White, K. L., Chen, J. M., Margot, N. A., Wrin, T., Petropoulos, C. J., Naeger, L. K. *et al.* (2004). Molecular mechanisms of tenofovir resistance conferred by human immunodeficiency virus type 1 reverse transcriptase containing a diserine insertion after residue 69 and multiple thymidine analog-associated mutations. *Antimicrob. Agents Chemother.* **48**, 992–1003.

25. Matamoros, T., Franco, S., Vazquez-Alvarez, B. M., Mas, A., Martinez, M. A. & Menendez-Arias, L. (2004). Molecular determinants of multi-nucleoside analogue resistance in HIV-1 reverse transcriptases containing a dipeptide insertion in the fingers subdomain: effect of mutations D67N and T215Y on removal of thymidine nucleotide analogues from blocked DNA primers. *J. Biol. Chem.* **279**, 24569–24577.
26. Gu, Z., Gao, Q., Faust, E. A. & Wainberg, M. A. (1995). Possible involvement of cell fusion and viral recombination in generation of human immunodeficiency virus variants that display dual resistance to AZT and 3TC. *J. Gen. Virol.* **76**, 2601–2605.
27. Huang, H., Chopra, R., Verdine, G. L. & Harrison, S. C. (1998). Structure of a covalently trapped catalytic complex of HIV-1 reverse transcriptase: implications for drug resistance. *Science*, **282**, 1669–1675.
28. Liu, S., Abbondanzieri, E. A., Rausch, J. W., Le Grice, S. F. & Zhuang, X. (2008). Slide into action: dynamic shuttling of HIV reverse transcriptase on nucleic acid substrates. *Science*, **322**, 1092–1097.
29. Rigby, S. T., Van Nostrand, K. P., Rose, A. E., Gorelick, R. J., Mathews, D. H. & Bambara, R. A. (2009). Factors that determine the efficiency of HIV-1 strand transfer initiated at a specific site. *J. Mol. Biol.* **394**, 694–707.
30. Rigby, S. T., Rose, A. E., Hanson, M. N. & Bambara, R. A. (2009). Mechanism analysis indicates that recombination events in HIV-1 initiate and complete over short distances, explaining why recombination frequencies are similar in different sections of the genome. *J. Mol. Biol.* **388**, 30–47.
31. Operario, D. J., Balakrishnan, M., Bambara, R. A. & Kim, B. (2006). Reduced dNTP interaction of human immunodeficiency virus type 1 reverse transcriptase promotes strand transfer. *J. Biol. Chem.* **281**, 32113–32121.
32. Balakrishnan, M., Roques, B. P., Fay, P. J. & Bambara, R. A. (2003). Template dimerization promotes an acceptor invasion-induced transfer mechanism during human immunodeficiency virus type 1 minus-strand synthesis. *J. Virol.* **77**, 4710–4721.
33. Gao, L., Hanson, M. N., Balakrishnan, M., Boyer, P. L., Roques, B. P., Hughes, S. H. *et al.* (2008). Apparent defects in processive DNA synthesis, strand transfer, and primer elongation of Met-184 mutants of HIV-1 reverse transcriptase derive solely from a dNTP utilization defect. *J. Biol. Chem.* **283**, 9196–9205.
34. Wisniewski, M., Balakrishnan, M., Palaniappan, C., Fay, P. J. & Bambara, R. A. (2000). Unique progressive cleavage mechanism of HIV reverse transcriptase RNase H. *Proc. Natl Acad. Sci. USA*, **97**, 11978–11983.
35. Peliska, J. A. & Benkovic, S. J. (1992). Mechanism of DNA strand transfer reactions catalyzed by HIV-1 reverse transcriptase. *Science*, **258**, 1112–1118.
36. Purohit, V., Roques, B. P., Kim, B. & Bambara, R. A. (2007). Mechanisms that prevent template inactivation by HIV-1 reverse transcriptase RNase H cleavages. *J. Biol. Chem.* **282**, 12598–12609.
37. Purohit, V., Balakrishnan, M., Kim, B. & Bambara, R. A. (2005). Evidence that HIV-1 reverse transcriptase employs the DNA 3′ end-directed primary/secondary RNase H cleavage mechanism during synthesis and strand transfer. *J. Biol. Chem.* **280**, 40534–40543.
38. Wisniewski, M., Balakrishnan, M., Palaniappan, C., Fay, P. J. & Bambara, R. A. (2000). The sequential mechanism of HIV reverse transcriptase RNase H. *J. Biol. Chem.* **275**, 37664–37671.
39. Lin, Y., Nieuwlandt, D., Magallanez, A., Feistner, B. & Jayasena, S. D. (1996). High-affinity and specific recognition of human thyroid stimulating hormone (hTSH) by *in vitro*-selected 2′-amino-modified RNA. *Nucleic Acids Res.* **24**, 3407–3414.
40. DeStefano, J. J., Bambara, R. A. & Fay, P. J. (1993). Parameters that influence the binding of human immunodeficiency virus reverse transcriptase to nucleic acid structures. *Biochemistry*, **32**, 6908–6915.
41. Yusa, K., Kavlick, M. F., Kosalaraksa, P. & Mitsuya, H. (1997). HIV-1 acquires resistance to two classes of antiviral drugs through homologous recombination. *Antiviral Res.* **36**, 179–189.
42. Sarafianos, S. G., Marchand, B., Das, K., Himmel, D. M., Parniak, M. A., Hughes, S. H. & Arnold, E. (2009). Structure and function of HIV-1 reverse transcriptase: molecular mechanisms of polymerization and inhibition. *J. Mol. Biol.* **385**, 693–713.
43. Beard, W. A., Bebenek, K., Darden, T. A., Li, L., Prasad, R., Kunkel, T. A. & Wilson, S. H. (1998). Vertical-scanning mutagenesis of a critical tryptophan in the minor groove binding track of HIV-1 reverse transcriptase. Molecular nature of polymerase–nucleic acid interactions. *J. Biol. Chem.* **273**, 30435–30442.
44. Roda, R. H., Balakrishnan, M., Hanson, M. N., Wohrl, B. M., Le Grice, S. F., Roques, B. P. *et al.* (2003). Role of the reverse transcriptase, nucleocapsid protein, and template structure in the two-step transfer mechanism in retroviral recombination. *J. Biol. Chem.* **278**, 31536–31546.
45. Delviks-Frankenberry, K. A., Nikolenko, G. N., Boyer, P. L., Hughes, S. H., Coffin, J. M., Jere, A. & Pathak, V. K. (2008). HIV-1 reverse transcriptase connection subdomain mutations reduce template RNA degradation and enhance AZT excision. *Proc. Natl Acad. Sci. USA*, **105**, 10943–10948.
46. Raja, A. & DeStefano, J. J. (2003). Interaction of HIV reverse transcriptase with structures mimicking recombination intermediates. *J. Biol. Chem.* **278**, 10102–10111.
47. Weiss, K. K., Bambara, R. A. & Kim, B. (2002). Mechanistic role of residue Gln151 in error prone DNA synthesis by human immunodeficiency virus type 1 (HIV-1) reverse transcriptase (RT). Pre-steady state kinetic study of the Q151N HIV-1 RT mutant with increased fidelity. *J. Biol. Chem.* **277**, 22662–22669.